

JGR Atmospheres

RESEARCH ARTICLE

10.1029/2017JD028079

Key Points:

- Polar lows can be associated with strong winds
- Polar lows can produce waves of 8 m or more
- PL characteristics (diameter, velocity, and atmospheric environment) explain the large intercase differences

Correspondence to:

M. Rojo,
maxence.rojo@lmd.polytechnique.fr

Citation:

Rojo, M., Claud, C., Noer, G., & Carleton, A. M. (2019). In situ measurements of surface winds, waves, and sea state in polar lows over the North Atlantic. *Journal of Geophysical Research: Atmospheres*, 124, 700–718. <https://doi.org/10.1029/2017JD028079>

Received 21 NOV 2017

Accepted 16 DEC 2018



Accepted article online 22 DEC 2018

Published online 26 JAN 2019

©2018. The Authors.

This is an open access article under the terms of the Creative Commons Attribution-NonCommercial-NoDerivs License, which permits use and distribution in any medium, provided the original work is properly cited, the use is non-commercial and no modifications or adaptations are made.

In Situ Measurements of Surface Winds, Waves, and Sea State in Polar Lows Over the North Atlantic

M. Rojo^{1,2} , C. Claud³ , G. Noer⁴, and A. M. Carleton⁵

¹Cultures, Environnements, Arctique, Représentations, Climats, Observatoire de Versailles Saint-Quentin, Guyancourt, France, ²Laboratoire Atmosphères, Milieux, Observations Spatiales, CNRS, Guyancourt, France, ³LMD/IPSL, CNRS UMR 8539, École Polytechnique, Université Paris Saclay, ENS, PSL Research University, Sorbonne Universités, UPMC Université Paris 06, Palaiseau, France, ⁴The Norwegian Meteorological Institute, Oslo, Norway, ⁵Department of Geography and The Polar Center, Pennsylvania State University, University Park, PA, USA

Abstract Polar low (PL) storms are an important feature of the wintertime subsynoptic-scale atmospheric circulation of middle- and higher-latitude ocean areas. They can generate hazardous conditions impacting coastal and marine activities like fishing, transport, and oil extraction. However, there are few studies available of individual PL systems based on high-resolution maritime surface data. Accordingly, the meteorological impacts of 29 PLs have been investigated for the 14 winters 1999–2013, using in situ measurements at eight stations in the Norwegian and North Seas. On average, the highest wind speed and significant wave height (SWH) occur following the minimum in sea level pressure of the PL, respectively, 1 and 3 hr after its passage. The strongest wind speed averages 17.1 m/s, and the highest peak SWH is 6.3 m, but these can reach 31 m/s and 11 m, respectively. PL characteristics of system horizontal extent, propagation speed, and the larger-scale atmospheric circulation environment explain the large intercase differences. Large, multiple, and fast-moving PLs within a meridional circulation environment appear to generate stronger near-surface winds and higher waves than do small, single, and slow-moving PLs within a zonal circulation. Multiple systems may have the largest impacts (e.g., SWH > 8 m), although a larger sample size is required to confirm this possibility. The impacts of PLs on sea surface temperature (SST) are quite small and are difficult to interpret separate from the background SST variation. The observed SST decrease may be mainly caused by the cold air outbreak within which the PL is embedded; indeed, a positive SST minus air temperature anomaly is found during the 24 hr preceding the passage of PL vortices, indicating enhanced low-level atmospheric instability.

1. Introduction

Over ice-free seas of higher latitudes, polar mesoscale cyclones occur preferentially during the cold season in the Northern Hemisphere and throughout the year in the Southern Hemisphere. The most intense of these systems is called polar lows (PLs; Rasmussen & Turner, 2003), which are defined as adopted in the present study: “A polar low is a small but fairly intense low in cold air outbreaks (CAO) well north of the polar front, with a cyclonic cloud structure and a diameter of 200–600 km” (Heinemann & Claud, 1997; Noer et al., 2011). This definition excludes larger dissipating extratropical cyclones, weak waves, and surface troughs. Often, several PLs and mesocyclones can form at the same time or successively in relative proximity.

Although PLs occur on relatively small spatial and temporal scales (a few hours to a few days) and have limited vertical extent (about 1 to 5 km), they can generate hazardous conditions that impact coastal and marine activities of fishing, transport, or oil extraction. Heavy snow and hail showers, strong wind gusts and squalls, and high waves and icing are also often associated with these more intense systems (e.g., Dysthe & Harbitz, 1987).

Notwithstanding, there are relatively few studies of the maritime conditions associated with PLs. Dysthe and Harbitz (1987) studied the effects of PLs on sea state conditions through use of a theoretical model and observations from a maritime weather station. Eidsvik (1987) applied autoregressive models on PL trajectories to estimate the hazard area and hazard probability of these systems. Claud et al. (1993, 2004) analyzed surface winds and significant wave heights (SWHs) for a PL using the satellite instruments Special Sensor Microwave/Imager, and Geosat altimeter, along with in situ measurements from buoys and the weather ship “Mike.” Sætra et al. (2008) investigated the possibility of sea surface warming due to intense vertical mixing in the upper ocean and entrainment of subsurface warm water, induced by the strong surface winds from

PLs, including observations during a PL event (17–18 December 2004). Isachsen et al. (2013) studied the sea surface response to a cold air outbreak (CAO) and PLs by allying numerous PL tracks from satellite observations (Operational Sea Surface Temperature and Sea Ice Analysis, and the Envisat altimeter) and surface drifter observations. Orimolade et al. (2016) estimated SWHs associated with PLs using a one-dimensional parametric wave model and compared the measured and the forecast SWHs for two PL cases in the Barents Sea. This study showed that PLs might induce large SWHs and that the key parameters are the PL propagation speed, its horizontal extent, and the associated surface wind speed (WS).

Despite these studies, which provide essential information for the present work, even fewer PL events have been documented using in situ measurements (just 13 events in the 30 years 1987–2016). Although Dysthe and Harbitz (1987) studied eight cases using a maritime weather station, only one PL—in February 1978—is described in detail. Similarly, the studies by Claud et al. (1993, 2004) and Saetra et al. (2008) each analyzed only a single PL using conventional observations, and Orimolade et al. (2016) presented two PL cases from December 2015.

The analysis of a greater number of PL events, relying on the same methods and data, can help validate and amplify those previous results. Such an analysis also provides a better sense of the range of PL impacts on WS, SWH, and sea surface temperature (SST). Potentially, information on WS and SWH may be useful for risk management and hazard reduction strategies. Indeed, small fishing boats of 15 m or less are particularly vulnerable to waves bigger than 5 m and to high winds. Also, certain operations on oil and gas platforms—especially those involving helicopters and cranes—are sensitive to sudden changes of atmospheric pressure and wind direction and to strong winds exceeding 15 m/s and gusts, wave heights greater than 5 m, and low visibility resulting from intense precipitation, hail, fog, icing, and lightning. Therefore, the scarce information available on the impacts of a larger sample of PLs on maritime conditions is a key motivator of this study.

This paper presents an analysis of the impacts of 29 PLs on near-surface WS, SWH, air temperature (AT), and SST conditions for the North and Norwegian Seas spanning the 14 winters 1999–2013. The time period is dictated by the availability of a detailed listing of PL events for the studied region.

The structure of the paper is as follows. Section 2 describes the data and methods of analysis. In section 3 we present the results of the climatic-scale analyses of the 29 PLs, followed by four case studies of the most intense PLs during the study period. Then, in section 4 we discuss the results and their significance. A summary of the results comprises section 5.

2. Data and Methods of Analysis

An analysis of in situ surface observations is used to determine the sea state associated with the PLs under consideration. First, the climatological attributes of PLs were analyzed by tracking their vortices on satellite imagery from their associated cloud signatures; this approach permits a relatively precise manual tracking for higher-latitude ocean regions (e.g., in Fitch & Carleton, 1991; Carleton, 1995). We note that, on average, satellite images are available every 3 hr (Rojo et al., 2015). Then, coincident observations of PL locations along their tracks and available maritime stations are identified.

Satellite-derived ocean WS data are not utilized here because the cloud liquid water content typically accompanying PLs adversely affects the accuracy of the retrievals (Claud et al., 1993; Draper & Long, 2004; Hilburn et al., 2006; Moore et al., 2008; Weissman & Bourassa, 2008; Renfrew et al., 2009; Weissman et al., 2012). Manual tracking of PLs on the satellite images is used (after Rojo et al., 2015) rather than an automated detection algorithm applied to reanalysis data because of the documented problem of poor or inconsistent representations of PLs in reanalyses (Laffineur et al., 2014; Zappa et al., 2014).

Because this paper aims to better understand the impacts of PLs on sea conditions to help mitigate the risks for maritime activities, and given that PLs affect a relatively wide area surrounding their centers, we analyzed separately the observations at the most affected stations and, thereafter, all available observations at those stations experiencing a substantial increase of WS or SWH and decrease of mean sea level pressure (SLP) from these events.

As described more fully in sections 2.1–2.3, below, 29 PL events reaching maritime stations in the vicinity of the Norwegian coast (i.e., 100–200 km from the coastline) for the 14 winters have been identified, and key

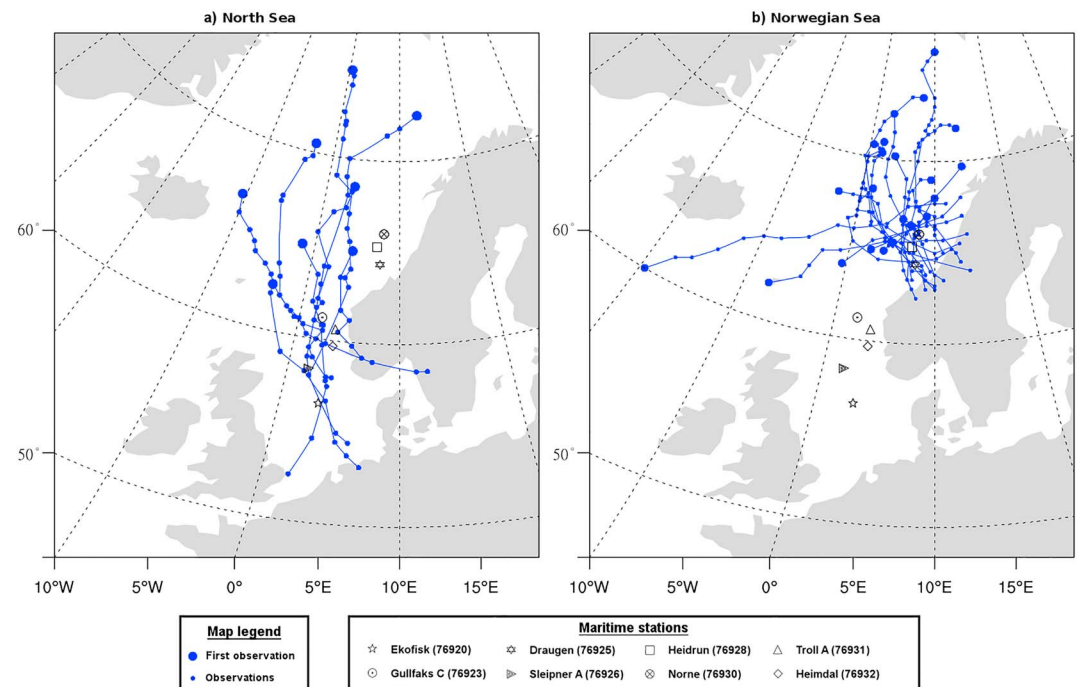


Figure 1. Positions of maritime stations and tracks of polar lows crossing one or more such stations in the winters of 1999–2013, for (a) North Sea and (b) Norwegian Sea.

variables in the available atmospheric and oceanic fields have been analyzed as the following data sources: (1) an annual listing of all PLs developed by the Norwegian Meteorological Institute (MET-Norway; Noer et al., 2011), (2) satellite imagery, and (3) observational data from maritime stations provided by MET-Norway.

2.1. PL Tracks

The PL tracks and system characteristics (cloud form, types, and sizes) are based on the annual listing of all PL activity since 1999. This list covers an area extending from the Greenland east coast to Novaya Zemlya in longitude and from 65°N to the Arctic ice edge in latitude. It gives the date and position for a single location of 190 PLs at the mature stage (i.e., one location per PL), defined as being when the cloud structure displays a pronounced vortex with cloud free eye, for the period September 1999 to May 2013. The list also provides the minimum SLP and the maximum near-surface WS of PLs for which those data are available.

Based on this PL list, all 190 events occurring in the 14 winters were tracked, following the procedure described in Rojo et al. (2015). From those events, 29 PLs (Figure 1) impacted directly one or more maritime stations (see below); accordingly, these 29 events are studied in detail using the in situ surface observations.

2.2. Maritime Stations

Assessing the maritime impacts of PLs relies on atmospheric and oceanic data also provided by MET-Norway (<http://eklima.met.no>). Three maritime stations in the Norwegian Sea and four in the North Sea are available for the full study period (Table 1), providing data at 20-min intervals on the following variables: SWH, SLP, and the WS at 10 m above the surface, AT at 10 m, and SST.

2.3. Methods

Our analysis of WS, SWH, SLP, AT, and SST (section 3.1) includes only one record per PL event (29 PLs), that is, the record coinciding with the time of minimum SLP at closest approach to a given station (hereafter referred to as the reference time). Observations included in the analysis comprise the gray highlighted portions of Table 2. About 20% of the SST data are missing, which reduces the number of PL coincidences with the surface observations.

All but one of the 29 selected PLs affect the maritime conditions at more than one station. For this reason, the maximum WS and peak SWH (section 3.2) have been analyzed considering all affected stations (95

Table 1
List of Maritime Stations Available for the North and Norwegian Seas

Station	Station #	Latitude (°N)	Longitude (°E)	Available from	WS (m/s)	SLP (hPa)	AT (°C)	SST (°C)	SWH (m)
Norne	76930	66,03	8,09	Oct 1995	Yes	Yes	Yes	<u>Yes</u>	Yes
Heidrun	76928	65,32	7,32	Feb 1998	Yes	Yes	Yes	<u>No</u>	Yes
Draugen	76925	64,35	7,78	Oct 1993	Yes	Yes	Yes	<u>Yes</u>	Yes
Gullfaks C	76923	61,2	2,27	Nov 1989	Yes	Yes	Yes	<u>Yes</u>	Yes
Troll A	76931	60,64	3,72	Jan 1998	Yes	Yes	Yes	<u>No</u>	Yes
Heimdal	76932	59,57	2,23	Jan 2003	Yes	Yes	Yes	<u>Yes</u>	Yes
Sleipner A	76926	58,37	1,91	Oct 1993	Yes	Yes	Yes	<u>No</u>	Yes
Ekofisk	76920	56,55	3,21	Jan 1980	Yes	Yes	Yes	<u>Yes</u>	Yes

Note. Underlined text shows the variables that are often missing. WS = wind speed; SLP = sea level pressure; AT = air temperature; SST = sea surface temperature; SWH = significant wave height.

records, Table 2). We categorize PLs according to the cloud vortex diameter, the system speed of movement, and its synoptic environment (circulation pattern). The PL diameter is measured across the cloud vortex from due west to east. Note that the diameter of PLs can vary during their lifespan; for this study, the PL size when its center is closest to a maritime station.

The PL velocity is a 24-hr average spanning 12 hr before and after the reference time (sections 3.1 and 3.2). For events lasting less than 1 day, the average speed is calculated over the entire lifespan.

To clarify the association between PL maritime conditions and the larger-scale atmospheric environment, we categorized the observations of WS and SWH using the same classification of North Atlantic circulation modes as Mallet et al. (2013). These circulation modes are as follows: Atlantic Ridge (AR), Scandinavian Blocking (SB), NAO−, and NAO+. Note that measurements on two of the 29 PLs are not considered here because they occurred outside the period for which the associated weather regimes are well defined (November–March). PLs forming within AR and SB modes are classified as “meridional circulation,” and PLs forming within NAO− and NAO+ modes are classified as “zonal circulation” (Cassou et al., 2004).

To assess the statistical significance of the results of PL categories, the nonparametric Kolmogorov-Smirnov test is used because the data series do not necessarily follow a normal distribution.

3. PL Climate-Scale Results

3.1. Mean Impacts of PLs on Near-Surface WSs, SWH, 10-m AT, and SST

Figure 2 displays the average WS and SWH for the 29 PL events. The maximum WS occurs just after the time of minimum SLP. On average, the SLP decreases from 995 to 991 hPa in the 6 hr before the reference time, which corresponds to an average WS increase of 10 to 15 m/s. The average WS increases more abruptly 2 hr before the passage of the PL vortex over the station, strengthening from 12 to 14.5 m/s. After reaching its peak, the WS decreases rapidly and continuously thereafter (Figure 2).

The maximum SWH occurs, on average, more than 1.5 hr after the minimum in SLP. SWH starts to increase 3 hr before the reference time (time of minimum SLP) and builds continuously until reaching an average maximum height of 5.3 m. During this 5-hr period, the mean SWH increases by more than 1 m. SWH only begins to decrease 5 hr after the reference time. The average SWH remains higher than 5 m for 7 hr following the reference time.

Only the following events are considered in the analysis and compilation of the SST statistics (i.e., observations for 19 PLs):

- Station Ekofisk (76920): PL5, PL6, and PL8;
- Station Draugen (76925): PL10, PL12, PL13, PL20, and PL23;
- Station Norne (76930): PL2, PL3, PL9, PL 11, PL14, PL15, PL17, and PL29;
- Station Heimdal (76932): PL7, PL16, and PL26.

These stations were selected because they provide good temporal coverage of both AT and SST, allowing comparisons between both variables (e.g., SST minus AT). Concerning the coincident SST observations, the spread is very large and, consequently, is not reported on Figures 3, 11, and 12.

Table 2
List of PLs Impacting Maritime Station, Considered in This Study

No	Date	Station	Minimum MSLP time	Maximum WS	Maximum SWH
1	31/01/00	76925	08:00	31.5	7.2
	31/01/00	76928	08:00	17.7	6.5
	31/01/00	76930	09:00	21.5	6.4
2	12/11/01	76925	13:40	19.3	8.5
	12/11/01	76928	11:20	16.5	9.1
	12/11/01	76930	09:20	18.1	6.7
3	23/01/02	76925	10:40	12.2	3.8
	23/01/02	76928	07:00	15.6	3.8
4	23/01/02	76930	06:40	13.1	4.7
	25/01/02	76925	—	12.4	5.5
	25/01/02	76928	05:40	11.7	5.2
	25/01/02	76930	06:00	8.5	5
4bis	25/01/02	76925	16:40	12.2	5.3
	25/01/02	76928	14:40	14.9	4.9
5	25/01/02	76930	11:20	8.6	4.8
	23/02/02	76920	09:00	18	7.3
	23/02/02	76926	03:40	18.8	—
	23/02/02	76925	19:20	19.6	8.5
	23/02/02	76928	18:20	18.9	8.1
	23/02/02	76930	17:00	22.8	7.8
6	31/01/03	76920	04:40	16.9	7.2
	31/01/03	76926	02:00	21.5	7.7
7	31/01/03	76923	15:00	24.5	10.5
	31/01/03	76932	17:40	20.1	6.7
8	29/01/04	76920	00:00	16.6	6.8
	28/01/04	76923	05:40	17.3	5.5
	28/01/04	76926	21:00	21.4	6.9
9	28/01/04	76931	07:20	9.6	4.9
	28/01/04	76932	19:20	9.2	7.3
	22/02/04	76925	00:40	—	6.1
	22/02/04	76928	00:00	17.7	6.3
	21/02/04	76930	22:00	17.2	6.2
10	16/11/04	76925	04:20	18.1	6.4
	16/11/04	76928	01:00	12.6	6.7
11	11/12/04	76925	01:40	18.1	6
	11/12/04	76928	09:00	17.5	—
	11/12/04	76930	07:00	8.2	5
12	03/09/07	76925	04:20	18.2	5.4
	03/09/07	76928	01:40	16.6	5.7
	03/09/07	76930	01:00	17.8	4.9
13	04/03/08	76925	16:20	24.8	8.5
	04/03/08	76928	15:20	21.9	8
	04/03/08	76930	13:20	18.6	6.9
14	17/03/08	76925	11:20	14.8	5.1
	17/03/08	76928	09:20	13.7	5.6
	17/03/08	76930	07:40	10	5.7
15	19/03/08	76925	06:00	14.4	3.7
	19/03/08	76928	02:20	14.1	3.6
	19/03/08	76930	01:40	14.9	3.7
16	29/10/08	76920	14:00	13.1	5.2
	28/10/08	76923	14:20	17.8	5.8
	29/10/08	76926	06:00	16.1	6.2
	28/10/08	76931	18:00	18.8	5.3
	28/10/08	76932	16:20	16.1	7

Table 2 (continued)

No	Date	Station	Minimum MSLP time	Maximum WS	Maximum SWH
17	20/11/08	76928	12:40	25.7	11
	20/11/08	76930	11:40	24.8	10.2
17bis	21/11/08	76925	07:00	22.4	9.1
	21/11/08	76928	04:00	24.2	10.4
	21/11/08	76930	00:40	23.2	9
18	30/01/10	76925	08:20	14.6	4.5
	30/01/10	76928	03:00	13.8	5.8
	30/01/10	76930	00:00	18.8	4.9
19	30/01/10	76923	19:00	18.2	7.9
	31/01/10	76926	02:00	16.8	5.2
	30/01/10	76931	22:20	16.7	5.8
	31/01/10	76932	00:00	16.3	6
20	05/12/10	76925	11:00	18.3	5.5
	05/12/10	76928	10:20	15.4	4.6
	05/12/10	76930	16:40	13.4	3.4
21	07/12/10	76923	07:00	12.4	4.3
22	07/02/11	76925	16:20	18.1	6.4
	07/02/11	76928	13:40	16.3	5.5
	07/02/11	76930	14:00	15.4	4.5
23	12/03/11	76925	04:40	13.6	5.5
	12/03/11	76928	04:40	10.1	4.5
	12/03/11	76930	03:20	7.1	4
24	13/03/11	76928	11:00	13.7	3.6
	13/03/11	76930	13:40	15.5	3.2
25	22/03/11	76925	15:40	23.5	9.1
	22/03/11	76928	13:20	23.7	8.2
	22/03/11	76930	14:20	19.2	7
26	06/12/11	76920	13:00	18.8	6.8
	06/12/11	76923	05:40	13.4	5.1
	06/12/11	76926	09:20	20.9	7.2
	06/12/11	76931	08:40	15.8	5.6
	06/12/11	76932	10:20	17.8	4.9
27	10/03/12	76925	08:20	19.3	8
	10/03/12	76928	08:00	18.5	6.4
	10/03/12	76930	08:40	18.1	5.9
28	06/03/13	76925	01:00	21.3	6.3
	05/03/13	76928	23:20	20.3	6.4
	05/03/13	76930	23:40	19.5	7.2
29	07/03/13	76925	00:20	16.5	6.8
	07/03/13	76928	00:20	17.6	8
	06/03/13	76930	23:20	17	7.7

Note. High impact events (wind speed exceeding 23 m/s and significant wave height greater than 8.5 m) are displayed in red, and observations included in our statistics for mean impacts are highlighted in gray. MSLP = minimum sea level pressure; WS = wind speed; SWH = significant wave height.

On average, the AT decreases by more than 2 °C in the 24 hr preceding the PL passage, with the minimum occurring 6 hr before (Figure 3) and resulting in a large positive difference between the SST and AT (about 2 °C) in the period from 15 to 5 hr before the passage of PL, that is, low static stability and inferred upward fluxes of sensible and latent heat. Indeed, the SST decreases only slightly during the PL passage (Figure 3). The lowest SST occurs on average between 1 and 3 hr after passage of the center over the station. During this period, the SST declines by 0.2 °C on average. However, there is considerable PL variability around this mean SST value. For example, the available observations show almost no variation of SST during the passages of PL15 and PL29, an increase of SST before the reference times for PLs 2, 5, 9, 20, 25, and 26, slight

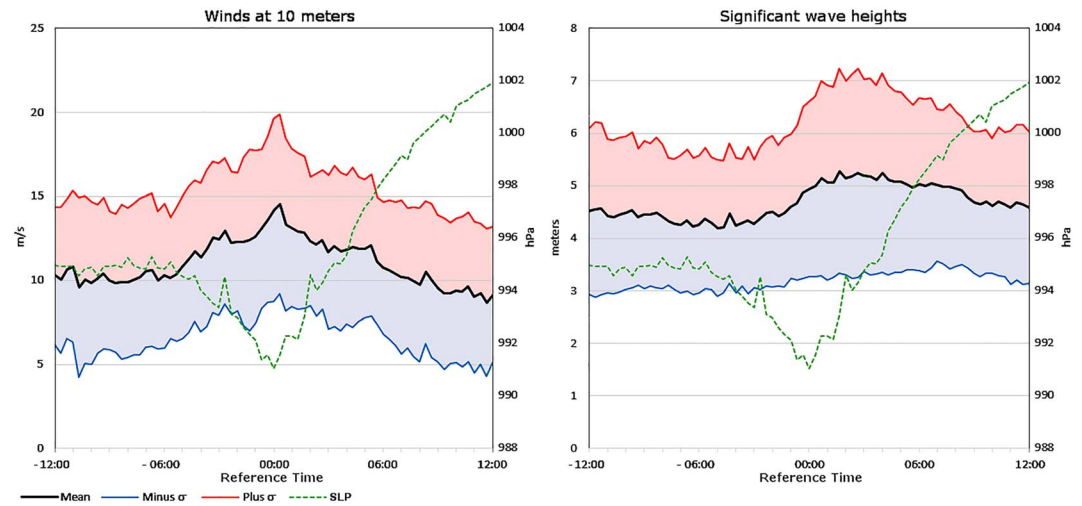


Figure 2. Mean and range standard deviations of wind speed and significant wave heights averaged for transits of 29 polar lows (refer text). The 00:00 reference time is the time of minimum sea level pressure (SLP).

decreases for PLs 3, 6, 8, 10, and 14, and stronger decreases of between 0.4 to 0.6 °C for PLs 7, 11–13, 16, 17, and 23 (not shown).

3.2. Station Measurements of Peak Winds and Waves at All Affected Stations

We next describe the impacts of PLs on maritime conditions at all affected stations (95 measurements on the 29 PL events, Table 2), specifically the observed peaks of WS and SWH. The overall mean peak WS is 17.1 m/s, occurring 1 hr after the minimum SLP (Figure 4a). A mean peak SWH of 6.3 m occurs 3 hr after the minimum SLP (Figure 4b).

These average values of PL associated WS and SWH conceal considerable variability (standard deviations of about 4 m/s for WS and 1.7 m for SWH); indeed, more than 20% of WS observations at the maritime stations are less than 14 m/s, while almost 20% exceed 20 m/s. Although more than 65% of the peak WS observations are recorded within ± 3 hr of the reference time, some PLs induce WS peaks more than 6 hr after passage of the vortex. Despite the wide range of PL impacts on WS and SWH, half of the peak wave heights occur within 4 hr following the SLP minimum, although some peak SWHs are recorded more than 10 hr after the reference time. The strongest SWH can also be observed starting 6 hr before the reference time, typically associated with the passage of the first cloud band accompanying the PL vortex (Figures 4a and 4b).

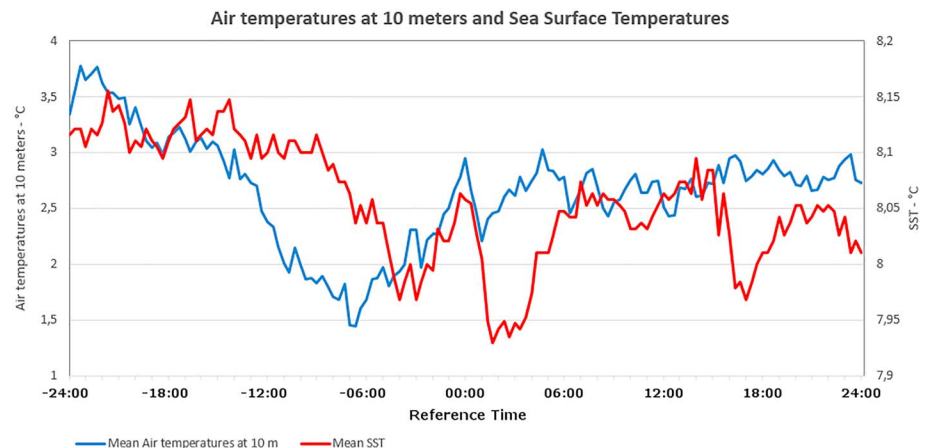


Figure 3. Mean sea surface temperature and air temperature during the transit of 12 polar lows. The reference time is the time of minimum sea level pressure. Note the different scales used for sea surface temperature (SST) and air temperature.

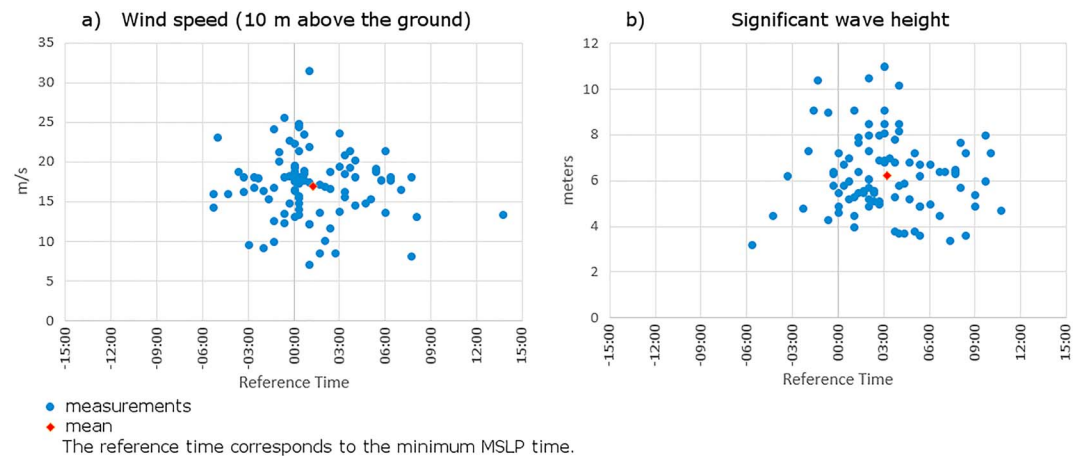


Figure 4. Peak wind speeds (a) and significant wave heights (b) for the 29 polar lows. The red rhombus indicates the mean value. The reference time corresponds to the time of minimum sea level pressure (MSLP).

This large range of PL maritime impacts likely reflects heterogeneity in the types of PL passage—whether vortex or cloud band, fast moving or quasi-stationary—and PL characteristics of size, stage of development, single or multiple vortices, and the associated synoptic pattern (e.g., the intensity of the prevailing CAO and circulation regime). Accordingly, to better interpret these composite results for the 29 PLs, we now undertake a more refined analysis that considers PL diameter, propagation speed, and the accompanying large-scale atmospheric environment.

3.2.1. Size

Two groups of PL diameter are defined: PLs smaller than or equal to 350 km and PLs larger than 520 km. These categories correspond, respectively, to the first and third quartiles of the total size distribution.

Figures 5a and 5b, and 6a and 6b categorize WS and SWH by PL diameter. PLs were distinguished as “small,” less than or equal to 350 km; and “large,” greater than 520 km. There are 28 measurements on 10 small PLs and 25 measurements on 9 large PLs. The impacts of PLs on WS and SWH are significantly different between both magnitude categories at greater than the 0.05 level (Tables 3 and 4). On average, large PLs are associated with higher mean peak WS (19 m/s) and peak SWH (6.8 m) than small PLs (15.6 m/s and 5.7 m, respectively). Indeed, WS peaks range from 8.6 to 23.7 m/s for the small PLs but from 10 to 31.5 m/s for the large PLs. Also, peaks of SWH range from 3.4 to 9.1 m for the small PLs and from 4.5 to 11 m for the large PLs (Figures 5a and 5b, and 6a and 6b).

3.2.2. PL Propagation Speed

Two groups of PL velocity are identified, each corresponding to the first and third quartiles of the distribution of PL propagation speed: PLs moving slower than 30 km/hr and PLs moving faster than 50 km/hr. There are 24 measurements on 10 PLs for PL velocities slower than or equal to 30 km/hr (8.33 m/s) and 23 measurements on 8 PLs for PL velocities faster than 50 km/hr. Figures 5c and 5d, and 6c and 6d display the significant differences (Kolmogorov-Smirnov test) between both sample distributions, respectively, p values of 0.001 and lower than 0.0001 (Tables 3 and 4).

The peaks of WS and SWH are highest when PLs move fast. The peak WS averages 14.7 and 19.1 m/s for the slow and fast categories of propagation speed, respectively. Similarly, the average peak SWH by PL propagation speed is 5 and 7.1 m. This result corroborates studies suggesting greater wave heights under faster-moving systems (e.g., Bowyer & MacAfee, 2005; Dysthe & Harbitz, 1987). The surface observations show large variability of PL impacts on the sea state. As given in Figures 5c and 5d and Table 3, the WS peaks range from 7.1 to 20.7 m/s for the slow PLs (standard deviation of 3.4 m/s) and from 9.2 to 31.5 m/s for fast PLs (standard deviation of 4.7 m/s). Also, peaks of SWH range from 3.2 to 7.2 m for slow PLs (standard deviation of 1 m) and from 4.5 to 11 m for fast PLs, with a standard deviation of 1.1 m (Figures 6c and 6d and Table 4).

We observe that, for PLs moving faster than 50 km/hr, all the peaks in SWH occur after passage of the vortex over the maritime station. Also, a considerably narrower range of time experiences the WS and SWH peaks when PLs are moving faster than 50 km/hr (about 9 hr, between −03:00 and 06:00 for WS and between 01:00

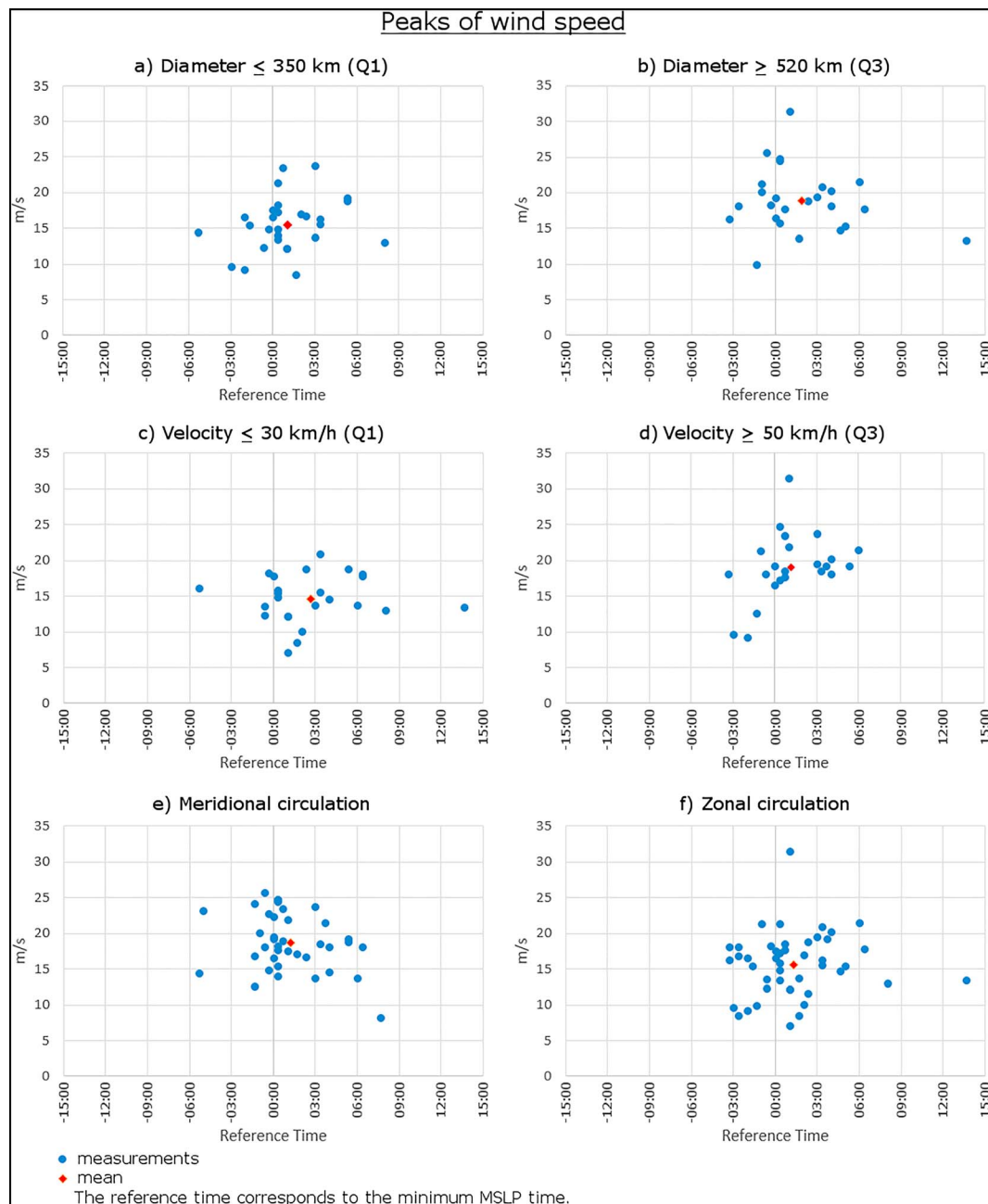


Figure 5. (a–f) Peak wind speeds in the west-east direction, the propagation speeds of 29 polar lows, and the synoptic circulation in which they are embedded. The red rhombus indicates the mean value. The reference time corresponds to the time of minimum sea level pressure (MSLP).

to 10:00 for SWH) than for PLs moving slower than 30 km/hr (about 19 hr for WS, between –05:00 and 14:00, and 17 hr for SWH, between –06:00 and 11:00).

3.2.3. Large-Scale Circulation

Categorizing the 27 cold-season PLs by their larger-scale circulation pattern reveals that 14 are embedded within meridional circulation (12 PLs forming within the AR mode and 2 PLs within the SB mode), and 13 PLs accompany zonal circulation (6 PLs within the NAO– mode and 7 PLs within the NAO+ mode). As shown in Tables 3 and 4, the wind and wave impacts of PLs on the maritime stations are significantly greater for meridional circulation than for zonal circulation (p values = 0.025 for WS, 0.005; Kolmogorov-Smirnov test). Thus, the peak WS averages 18.8 m/s for the meridional circulation patterns of AR and SB,

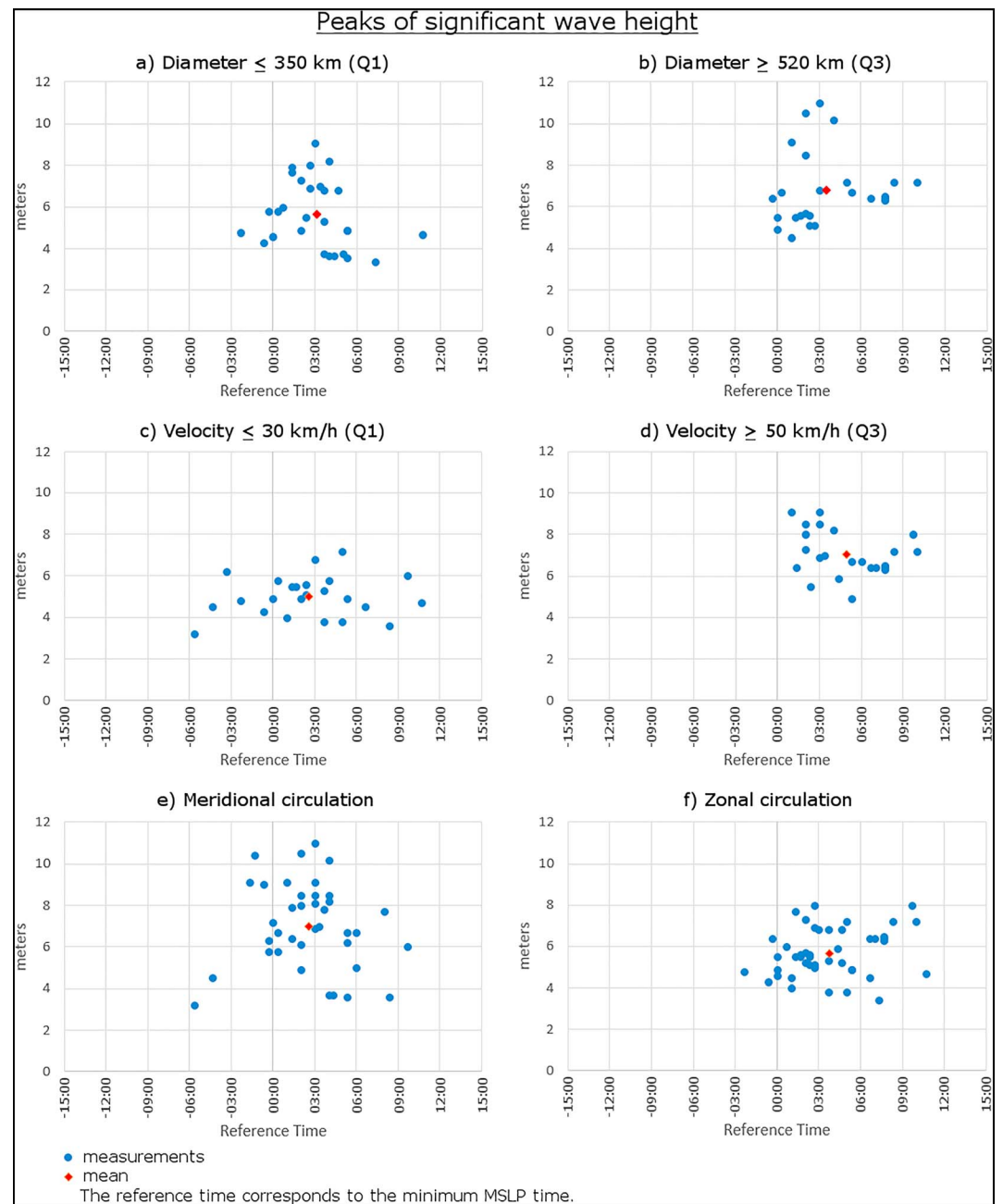


Figure 6. (a–f) Peak significant wave heights in the west-east direction, the propagation speeds of 29 polar lows, and the synoptic circulation in which they are embedded. The red rhombus indicates the mean value. The reference time corresponds to the time of minimum sea level pressure (MSLP).

but is only 16.2 m/s within zonal circulation (Figures 5e and 5f). Interestingly, the maximum WS value (31.5 m/s) is observed for a PL occurring within zonal circulation (Table 3). The WS observations are characterized by strong variability, with peaks ranging from 8.2 to 25.7 m/s (standard deviation of 4 m/s) for meridional circulation and from 7.1 to 31.5 m/s (standard deviation of 4.4 m/s) for zonal circulation. The average peak SWH exceeds 7 m for PLs occurring within meridional circulation but is only 5.7 m for PLs in zonal circulation (Figures 6e and 6f). Again, the variability around those mean values is large; 3.2 to 11 m (standard deviation of 2.1 m) for meridional circulation and 3.4 to 8 m (standard deviation of 1.1 m) for zonal circulation (Table 4).

Table 3
Descriptive Statistics of Peak WS and Nonparametric Kolmogorov-Smirnov Test of Their Distributions (Refer Text)

Peaks of wind speed (10 m above the ground)							
Descriptive statistics						Kolmogorov-Smirnov test	
Variable	Observations	Minimum	Maximum	Mean	σ	<i>p</i> value (bilateral)	Different ($\alpha = 0,05$)
Diameter < 350 km (Q1)	28	8.6	23.7	15,593	3,763	0.006	Yes
Diameter > 520 km (Q3)	25	10.0	31.5	18,964	4,488		
Velocity < 30 km/hr (Q1)	24	7.1	20.9	14,717	3,373	0.001	Yes
Velocity > 50 km/hr (Q3)	23	9.2	31.5	19,135	4,734		
Meridional	38	8.2	25.7	18,797	4,037	0.025	Yes
Zonal	46	7.1	31.5	15,663	4,440		

4. Results for High Impact PLs

Four PL events (denoted red in Table 2) are particularly strong, having a maximum WS greater than 23 m/s (approximately 83 km/hr) and a maximum SWH equal to or greater than 8.5 m. These thresholds correspond to the 90th percentile of the all PL WS and SWH observations. These intense cases are now described together, paying particular attention to their formation, movement characteristics, and associated atmospheric environment.

4.1. General Overview of Intense PLs

Similarities among the four most intense PLs also distinguish them from the other 25 PLs in the study sample. First, these four PLs are embedded within spatially and temporally extended CAO events having associated convection and instability, evident as “mostly open” convective cells and zones of convergence on satellite imagery (Figure 7), at the time of formation and subsequently.

Second, the four intense PLs develop at the southeastern edge of the CAO, within an area of strong temperature gradients, implying that these PLs deepen under the influence of both baroclinic and convective instability (Montgomery & Farrell, 1992).

Third, these intense PLs are not single events; rather, each comprises a cluster of several PLs and cold air mesocyclones, as follows:

- PL6 and PL7 merge to form a large system stretching 1,500 km from north to south and comprising two discreet mesoscale vortices and a long cloud band oriented along the Norwegian coast (Figures 7a, 7b, and 8a).
- PL13 is part of a multiple system accompanied by long cloud bands (Figures 7e, 7f, and 8b), which extends across about 1,500 km in the west-east direction and about 1,200 km from north to south.
- PL17 is embedded within a convective cloud field where three other PLs develop in succession (Figure 8c). This case is the only PL in our study period that has been classified as an extreme weather event by

Table 4
Descriptive Statistics of Peak SWH and Nonparametric Kolmogorov-Smirnov Test of Their Distributions (Refer Text)

Peaks of significant wave height							
Descriptive statistics						Kolmogorov-Smirnov test	
Variable	Observations	Minimum	Maximum	Mean	σ	<i>p</i> value (bilateral)	Different ($\alpha = 0,05$)
Diameter < 350 km (Q1)	28	3.4	9.1	5,686	1,635	0.040	Yes
Diameter > 520 km (Q3)	25	4.5	11.0	6,824	1,762		
Velocity < 30 km/hr (Q1)	24	3.2	7.2	5,029	0,999	<0.0001	Yes
Velocity > 50 km/hr (Q3)	23	4.9	9.1	7,091	1,107		
Meridional	38	3.2	11.0	7,042	2,080	0.005	Yes
Zonal	46	3.4	8.0	5,709	1,148		

Note. SWH = significant wave height.

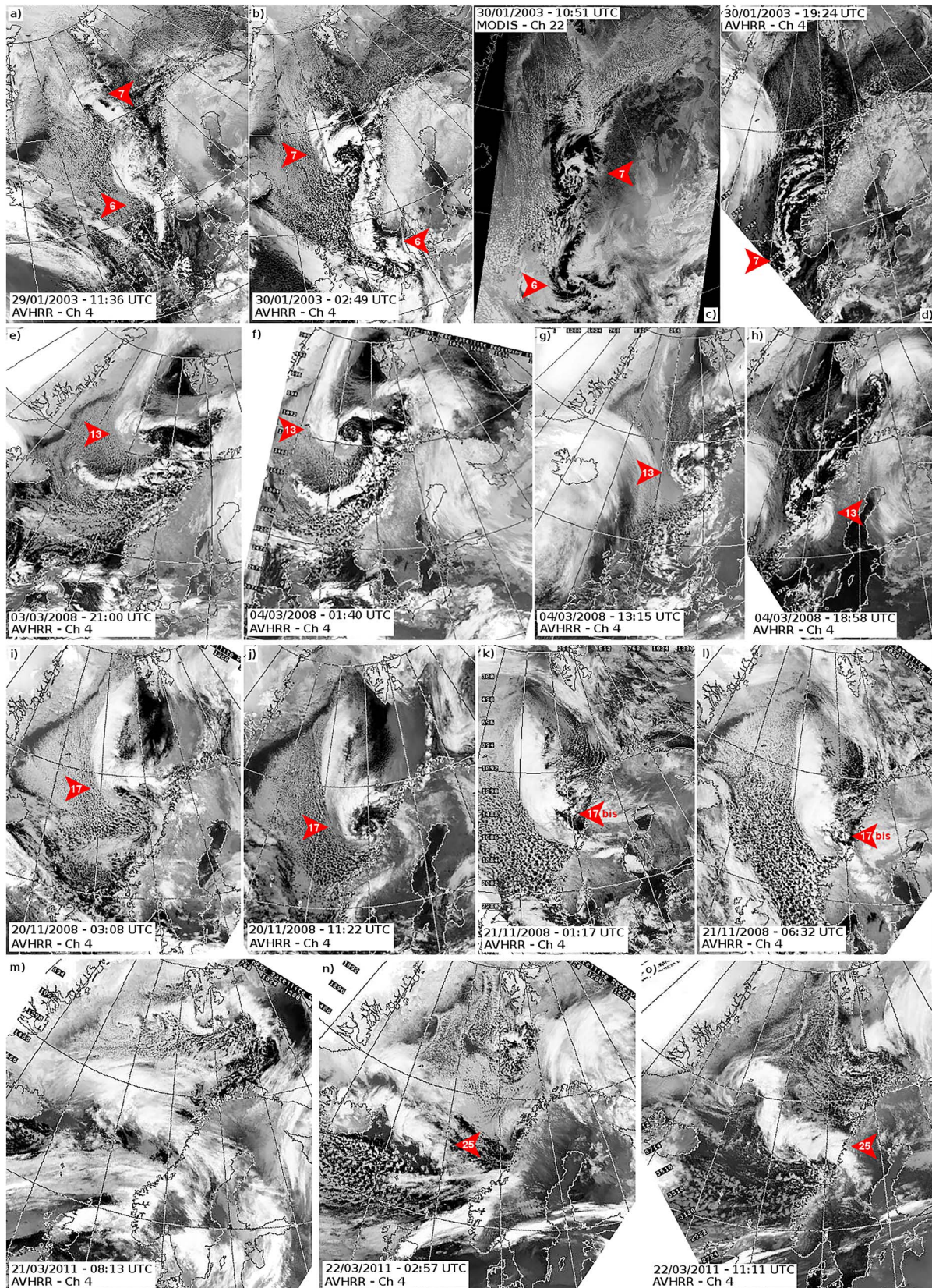


Figure 7. AVHRR thermal-infrared satellite images showing PL6 and PL7 (panels a–d), PL13 (panels e–h), PL17 (panels i–l), and PL25 (panels m–o). AVHRR = advanced very high resolution radiometer; MODIS = Moderate Resolution Imaging Spectroradiometer.

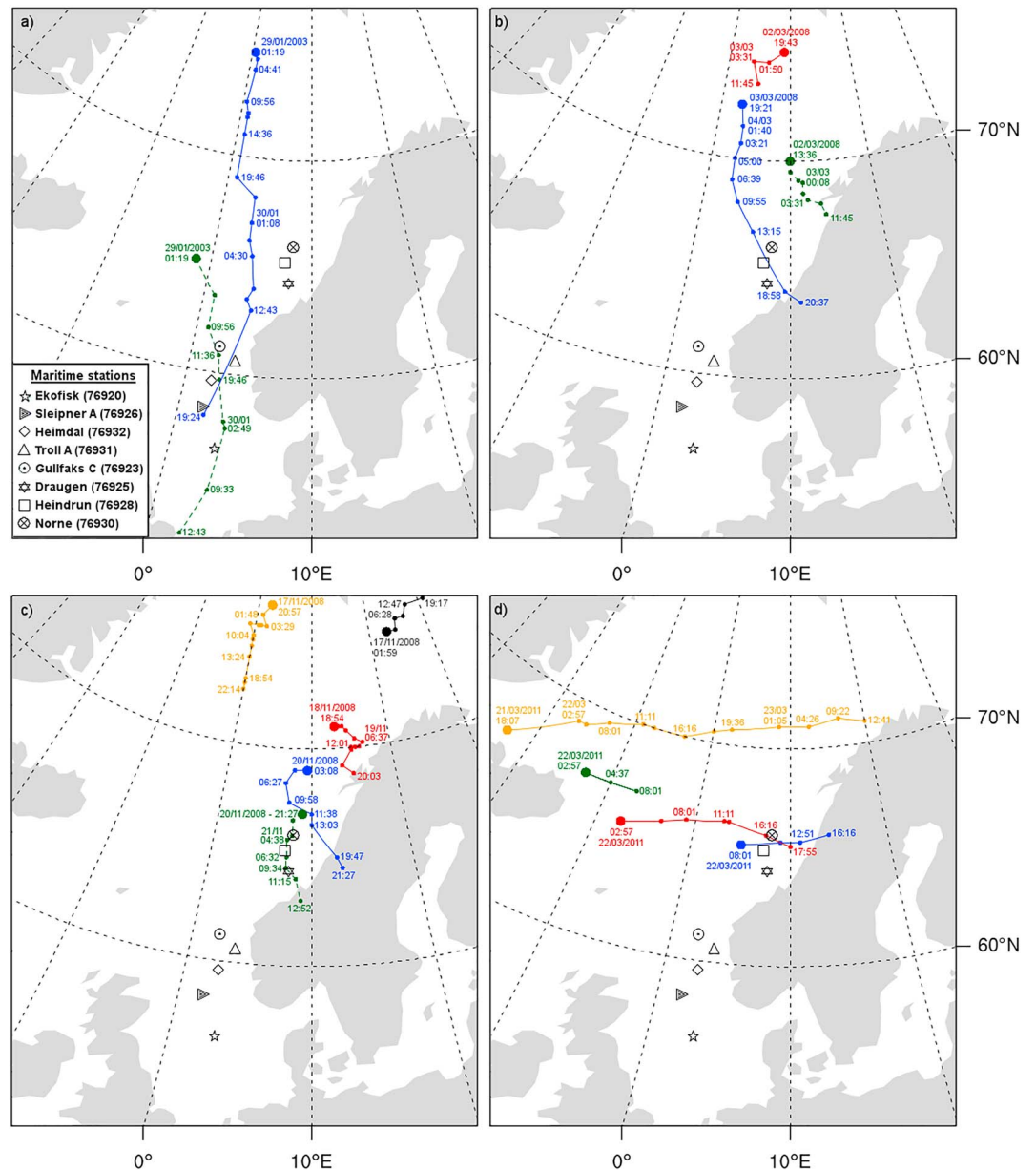


Figure 8. Individual tracks of intense polar lows (PLs); (a) PL6 in dashed green and PL7 in blue, (b) PL13 in blue, secondary systems in red and dashed green, (c) PL17 in blue, and PL17 reintensification in dashed green, secondary systems in red, black, and orange, and (d) PL25 in red, secondary systems in blue, green, and orange.

MET-Norway, when it was given the name Vera (Nordeng, 2009; Nordeng & Røsting, 2011). Vera has a diameter of about 600 km and is accompanied by a 1,000 km long cloud band.

- PL25 forms part of a multiple system (Figures 7n, 7o, and 8d) spanning about 1,200 km from west to east.
- Fourth, these four most intense PLs occur in already rough seas and relatively high winds resulting from the passage of the preceding synoptic lows or cold air mesocyclones and other PLs.

4.2. Intense PLs Affect a Relatively Wide Area

The observations at maritime stations indicate that PLs can impact a relatively large area. This assertion is particularly evident for the four strongest PLs, as represented by PL6 and PL7. PL6 passes over station Gullfaks C (North Sea) at maturity stage, on 29 January 2003 between 13:00 and 17:00 UTC

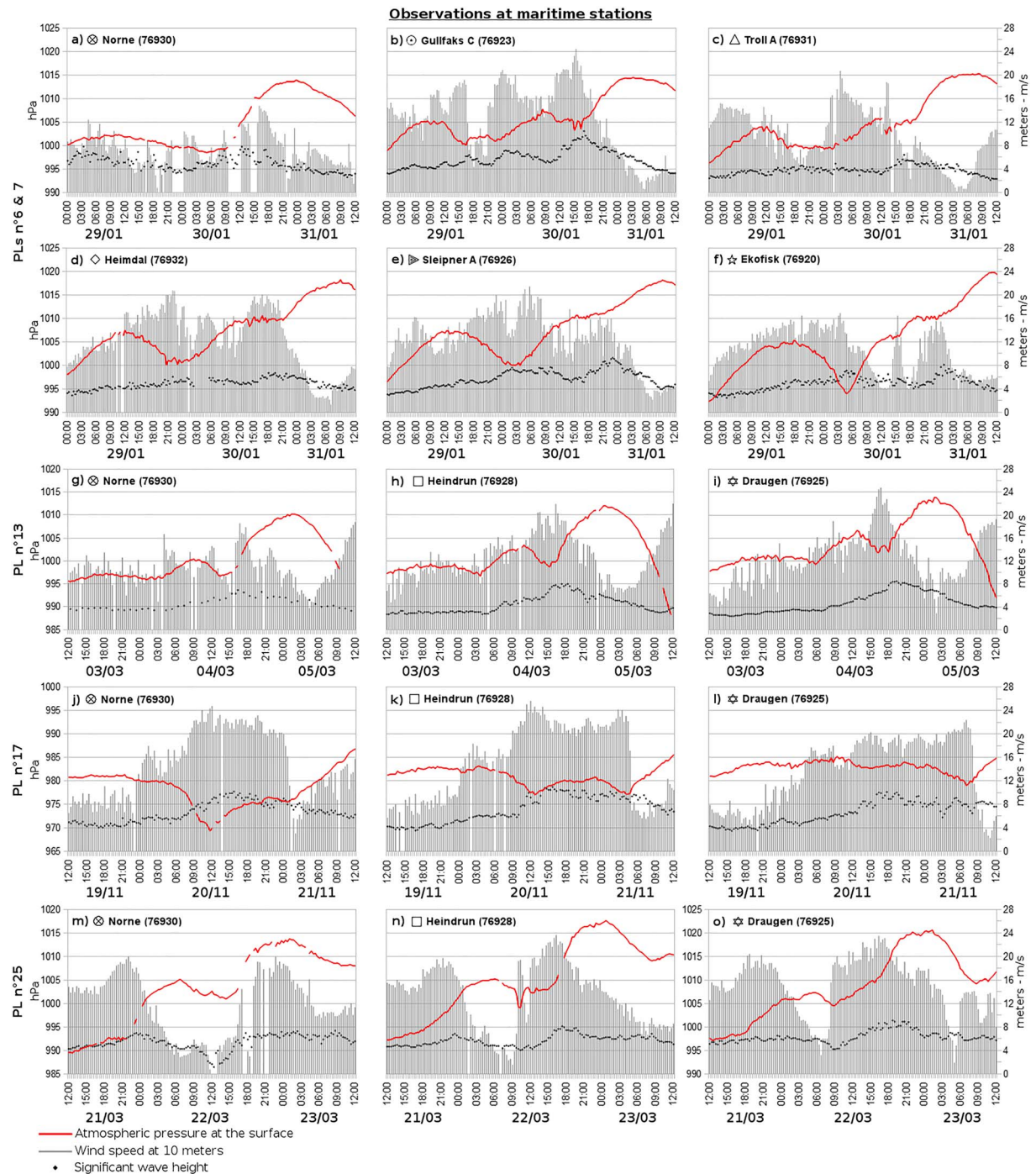


Figure 9. Wind speeds, significant wave heights, and sea level pressure records at marine stations. (a–f) Observations during PL6 and PL7, (g–i) observations during PL13, (j–l) observations during PL17, and (m–o) observations during PL25.

(SLP: 1,000.1 hPa at 16:20 UTC, WS: 19.2 m/s at 16:00 UTC, SWH: 6.4 m at 17:00 UTC; Figures 7b, 8a, 8b, and 9b). Subsequently, PL6 impacts station Heimdal, located 250 km further south, at 21:00 UTC (SLP: 1,000 hPa, WS: 21 m/s, SWH: 6 m; Figure 9d), and Sleipner A (SLP: 1,000 hPa at 02:00 UTC, WS: 20 m/s at 22:40 UTC, SWH: 7.6 m at 02:00 UTC; Figures 8a and 9e). Later still, PL6 affects station Ekofisk (about 500 km south of Gullfaks C) at 05:00 UTC (30 January) with the central SLP dropping to 994 hPa, the WS reaching 17 m/s and SWH of 7 m (Figure 9f).

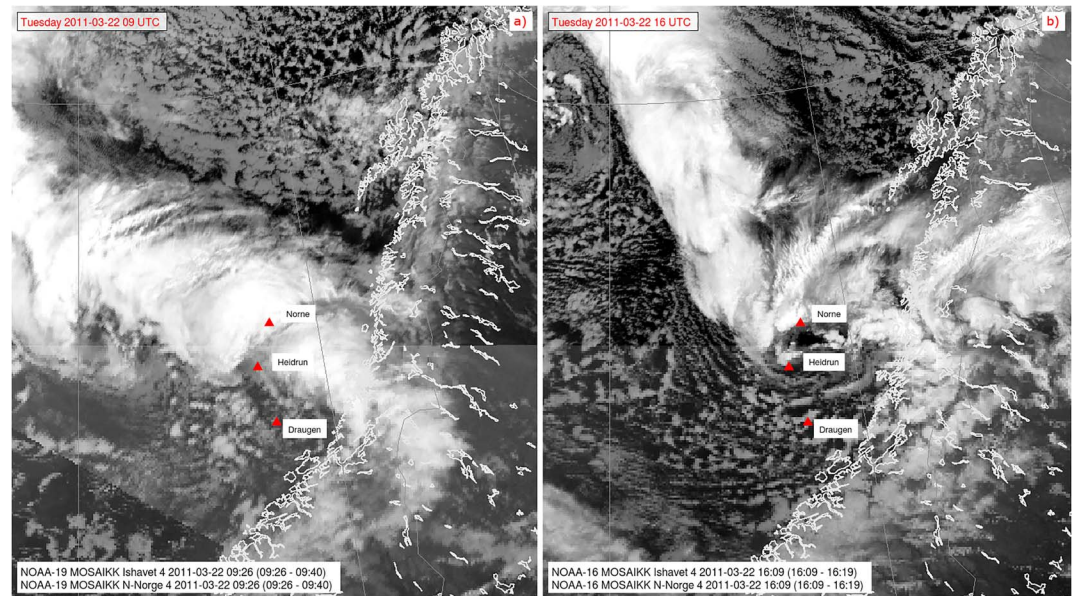


Figure 10. Satellite imagery illustrating the passage of PL25 over maritime stations in the Norwegian Sea. NOAA = National Oceanic and Atmospheric Administration.

In the Norwegian Sea, Norne station—located 600 km north of Gullfaks C—is impacted by PL7 and its cloud band on 30 January 2003 between 02:00 and 18:00 UTC (Figures 7b, 7c, 8a, and 9a). Although the maximum recorded WS is 14.8 m/s at 16:00 UTC (Figure 9a), there is also recorded a SWH increase of 4 m over 10 hr, from 3.7 m at 02:00 UTC to 7.8 m at 12:20 (Figure 9a). Indeed, these merged storms comprising PL6 and PL7 affect an area exceeding 6×10^5 km² (1,200 km north to south, 500 km east to west) during their life span.

4.3. Intense PLs Have Also Very Local Effects

A cluster of mesocyclones in which PL25 is embedded, develops north and east of Iceland on 22 March 2001, and subsequently affects three Norwegian Sea stations located to the eastward (Norne, Heidrun, and Draugen; Figures 7m–7o, 8d, 9m–9o, and 10).

During a first passage of PL 25, a strong lowering of SLP (6.1 hPa in 4 hr, reaching 999.2 hPa at 10:20 UTC) is observed at Heidrun. Gale-force winds are also recorded there (19.5 m/s at 10:20 UTC) and at Draugen (20.9 m/s at 11:20 UTC). At the same time, light winds are observed at Norne station (ranging from 1 to 6 m/s). During a second passage of this PL, maximum values of WS and SWH are recorded at Heidrun (23.7 m/s at 16:20 UTC and 8.2 m at 18:20 UTC) and at Draugen (23.5 m/s at 16:20 UTC and 9.1 m at 18:40 UTC). The Heidrun and Draugen stations are located in the southwest quadrant of the PL, where the gradient wind is in the same direction as the movement of the air mass in which the low is embedded.

Although the second passage of PL25 is most evident in the SLP at Norne (1,001 hPa at 14:20 UTC), no strong winds are observed there (4–7 m/s between 13:00 and 16:00 UTC). At this time, the Norne station—located on the north side—has the PL gradient wind more-or-less canceled out by the forward motion of the system. Norne is, for a short period, in the left rear quadrant of the low and then becomes immersed in the southern and more windy part of the low as the latter moves eastward. Starting at that time, Norne observes a rapid increase in SWH, from 1.2 to 7 m between 12:20 and 17:40 UTC.

The differences in wind and wave conditions among the three stations, which lie within 150 km of each other, illustrate that the direction from which the PL approaches a given location influences the rates of increase in the WS and SWH accompanying its passage.

4.4. A Cumulative Effect of PLs on Near-Surface WSs and SWH

The four strongest PLs, each being part of a larger system, impact the same area several times during their life span. The system formed by the merger of PL6 with PL7 impacts station Gullfaks C three times between 29 and 30 January 2003 (Figures 7d, 8a, and 9b). As displayed in Figure 9b, these station transits increase both the WS and SWH, as follows: for the first passage on 29 January 2003 at 09:00–12:00 UTC, the WS = 16.7 m/s, and SWH = 5.2 m; for the second passage at 15:00–17:00 UTC, WS = 19.2 m/s, SWH: 6.2 m; and for the third passage on 30 January 2003 at 12:00–18:00 UTC, WS = 24.5 m/s, SWH: 10.5 m. The movement of PL6 and PL7 over a wide area result in degraded sea state conditions that are maintained for approximately 36 hr.

The impact of PL13 on WS and SWH evidently is enhanced by the multiple PL system, with several secondary vortices forming in succession over a 48-hr period. Satellite images (Figures 7e and 7f) show a long cloud band in the vicinity of PL13, which affects all the stations in the Norwegian Sea on 4 March 2008 between 03:00 and 08:00 UTC. During this period also, stations record average winds of more than 16 m/s and waves of 4–5 m (Figures 9g–9i). Subsequently, between 15:00 and 18:00 UTC on 4 March 2008, PL13 impacts these same stations again (Figures 7g, 7h, and 8b). The SLP drops by approximately 4 hPa, and the WS increase attains short-time averages of 18.6 m/s at Norne, 21.9 m/s at Heidrun, and 24.8 m/s at Draugen. The SWH reaches 7.7 m at Norne, 8 m at Heidrun, and 8.5 m at Draugen (Figures 9g–9i).

Similar to PL 13, PL17 (Vera) is a multiple PL situation, albeit the strongest system of that cluster. On the first and last satellite images in the sequence showing the vortices accompanying Vera can be observed four separate PL systems over the Nordic Seas between 17 and 21 November 2008 (Figure 8c). At stations Norne, Heidrun, and Draugen the sea state is already degraded the day before Vera's passage, with waves reaching between 4 and 5 m. An earlier PL passes over the Lofoten archipelago (19 November 2008 at 20:00 UTC) generating a small peak of SWH (Figures 9j–9l). Subsequently, both SWH and WS increase steadily until the passage of Vera. When Vera reaches stations on 20 November 2008 at noon, the WS increases abruptly, as follows: at Norne to 24.8 m/s, at Heidrun to 25.7 m/s, and a lesser value of 20.3 m/s recorded at Draugen at 15:00 UTC. All three stations record an increase in SWH of at least 4 m over a 7-hr period (20 November 2008 between 09:00 and 16:00 UTC), reaching 11 m at Heidrun. Then, at the rear of its cloud band, Vera appears to reintensify (Figures 7k and 7l, and 9j–9l: an additional SLP decrease of 1–4 hPa on 21 November between 00:00 and 08:00 UTC). Subsequently, high winds and waves are observed, with WS exceeding 20 m/s and SWH reaching 8–10 m (Figures 9j–9l). At Norne, individual waves exceeding 20 m occur (not shown). The WS decreases immediately following Vera's passage, readily identifiable from the minimum SLP values at the three stations (975.5 hPa at Norne, 977.2 hPa at Heidrun, and 979.3 hPa at Draugen). Indeed, the WS at Norne decreases from 20 to 3.1 m/s between 00:00 and 02:00 UTC, at Heidrun it drops from 23.1 to 7 m/s between 04:00 and 05:00 UTC, and at Draugen it decreases from 20.9 to 5.3 m/s between 07:40 and 09:20 UTC (Figures 9j–9l). This sequence of multiple PLs strongly degrades sea state over the entire period, with maximum values of WS and SWH occurring during Vera's passage. The apparent reintensification of this PL maintains Norwegian Sea wave heights exceeding 8 m for almost 24 hr.

4.5. AT and SST Responses to Intense PLs

For the four intense PL cases considered together, there is a clear decrease in SST for 24–48 hr preceding the PL passage, at the stations situated within the CAO. On average, the SST decrease is greater for intense PLs than others. Figure 11 shows that an SST decrease exceeding 0.3 °C starts 13 hr before the minimum SLP occurs and finishes 12 hr after.

This feature indicates the SST is influenced by the strong cooling resulting from upward surface heat fluxes linked to the CAOs that precede the most intense PLs.

For AT, Figure 11 shows that, on average, this variable decreases by more than 3.5 °C in the 24 hr preceding the PL passage. The AT decrease is much greater for intense PLs than for less intense systems. Thus, the positive difference between the SST and AT is also larger (Figure 12). Indeed, the maximum SST minus AT value is about 7.4 °C for the most intense PLs and about 6.4 °C for all others. In both types of system, these maximum SST-AT differences are found 6 hr before the passage of the PL.

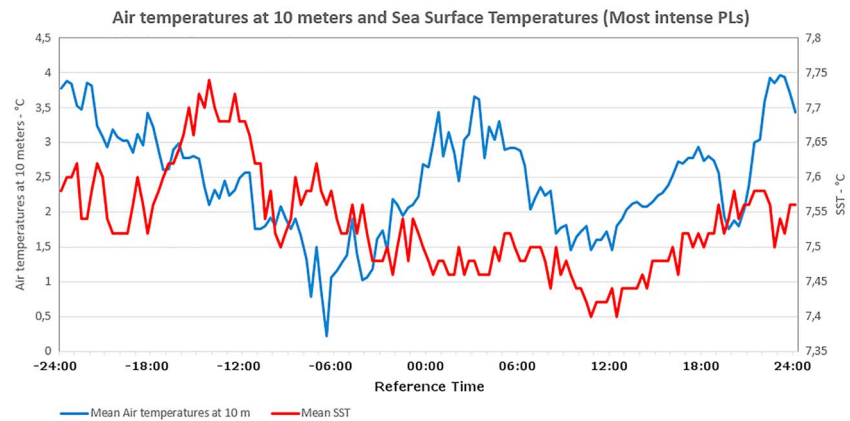


Figure 11. SSTs and air temperatures at maritime stations transited by intense PL events. The reference time is the time of minimum sea level pressure. Note the different scales used for SST and air temperature. PL = polar low; SST = sea surface temperature.

5. Discussion and Conclusions

The meteorological impacts of 29 PLs that intersected eight maritime stations in the Norwegian and North Seas over the 14 winters 1999–2013 have been investigated using both multicase (“climatic”) and case study approaches. In contrast with previous investigations, we use maritime surface observations of atmospheric variables (SLP, WS, and AT) and sea surface conditions (SWH and SST).

For the 29 PL cases considered together, the highest WS and SWH occur following the minimum in SLP, or reference time, by about 1 and 3 hr, respectively (Figure 3). This result agrees with Rasmussen and Turner (2003).

The peak WS averages 17 m/s, and the peak SWH averages 6.3 m. Peak WS values across the 29 PLs vary between 7 and 31 m/s, while SWH ranges between 3.2 to 11 m. These large intercase differences are explained by the large range in PL characteristics: their horizontal extent, their propagation speed, and the large-scale atmospheric circulation pattern in which they are embedded.

Individual maritime station measurements for four PL case periods selected on the basis of their higher system intensity show that, over their lifespan, strong PLs can impact an extended area (up to approximately $6 \times 10^5 \text{ km}^2$)—particularly for the observed wave heights—while also having locally strong winds.

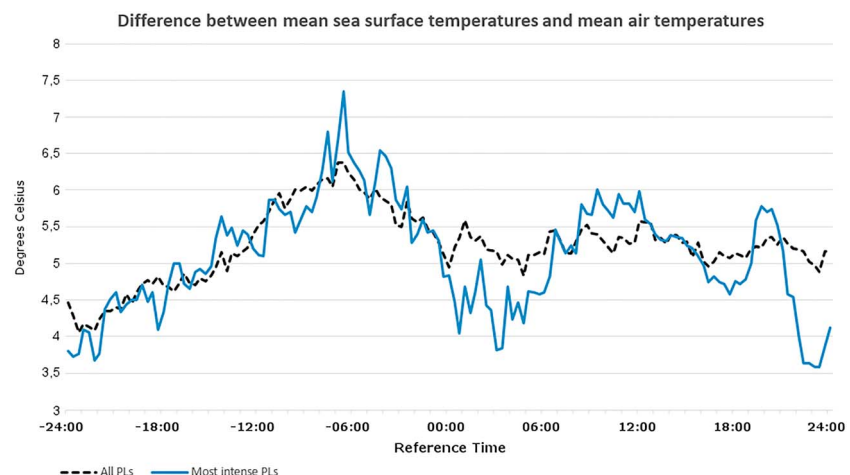


Figure 12. Differences between mean sea surface temperature and mean air temperature (i.e., sea surface temperature minus air temperature).

The direction from which a PL approaches a given station plays a key role in its local impact because the strongest winds typically are located in the system's southwestern quadrant: The gradient wind is in the same direction as the movement of the associated air mass (CAO). The cloud bands around PLs are associated with low-level convergence along shear lines between air streams on adjacent quadrants of the low (Claud et al., 2004). The sudden local changes in wind and waves across these shear lines are one of the most hazardous properties of a PL. There is a large statistical spread in the impacts across the distribution of PLs. The timing of the WS maxima can occur between 6 hr before to 15 hr after the minimum SLP, and the area affected is not always the same. These features are important for improving risk management of PL hazards.

Another key result of this study is that those PLs which are large, multiple, or fast moving and which are embedded within a larger meridional circulation environment generate, on average, stronger near-surface winds and higher waves than small, single, and slow-moving PLs occurring within more zonal circulation. Multiple and complex systems, often embedded within strong CAOs, may have the largest impacts on sea state. Indeed, strong CAOs favor the formation of PL clusters, affecting a wide area during a multiday period. The later PLs of a series form in already highly disrupted atmospheric boundary layer and upper ocean conditions, and so a cumulative effect on the sea state is observed. In such conditions, SWHs exceeding 8 m and individual waves exceeding 20 m occur (e.g., in "Vera").

The highest waves are observed in PLs having propagation speeds exceeding 50 km/hr. The reason might be that fast-moving PLs generally are embedded in a strong synoptic-scale gradient in SLP, with accompanying strong winds at the surface. According to Orimolade et al. (2016), fast-moving PLs do not favor dynamic fetch and enhanced wave growth because the PL tends to "outrun" the waves. Despite this possibility, it is to be expected that waves are affected by PLs not only through the locally strong gradient wind around the PL vortex but also by the strong synoptic-scale wind upstream of the PL.

Ocean waves can also "escape" the immediate PL environment to propagate downstream for slow-moving PLs and impact maritime stations before the arrival of the PL. The widest range of peak SWH in our sample is found for the slowest-moving PLs; for 25% of these systems, peak SWH arrives before or at the time of minimum-recorded SLP.

PL impacts on SST, and the latter's covariation with the AT, also differ widely: SST decreases are quite small (-0.2°C) and are particularly difficult to interpret separate from the background SST variation. The SST decrease begins, on average, 13 hr before the reference time. The fact that the AT decrease precedes that of the SST indicates the more immediate impact of the associated CAO and possibly also the effect of the stronger winds of the CAO inducing upwelling of colder water. The present study largely confirms the results of Isachsen et al. (2013) that the direct SST response to PLs is minimal because, by definition, a PL is relatively short lived. However, the SST minus AT metric is more informative as to the implied heat fluxes in the atmosphere's boundary layer for different sectors of a PL than is either the SST or AT separately. Indeed, a positive SST minus AT anomaly is observed during the 24 hr preceding the passage of the PL vortices, reaching a maximum 6 hr before the minimum SLP time. This positive difference between SST and AT is larger for the most intense PLs, suggesting that these PLs developed in a more unstable atmospheric environment with deeper convection and higher turbulent heat fluxes.

The physical interpretation of SST variations accompanying the passage of PLs should be done judiciously because our statistics are based on a relatively small sample (only 20 PLs out of 29 because of missing SST data). The large variation in the apparent response of the SST to PLs indicates that a more definitive assessment for this maritime variable requires a considerably larger sample of potential systems. It is also possible that the temporal frequency of the SST measurements, and sensitivity of the instruments to this variable, differs among stations, leading to biases. Finally, all stations used in this study are located relatively close to the Norwegian coast and the number of PL cases is still limited. Thus, no firm conclusions should be drawn about SST variations in PLs before a larger sample of events can be analyzed using measurements taken at more offshore stations, when these become available. Although satellite-retrieved passive microwave and scatterometer WSs can provide information over considerably larger scales than do surface stations, their value within PLs is limited by the relatively small size of these systems, the coarse spatial resolution of radiometric sensors, and the reduced accuracy within inclement weather and rough seas (Carleton et al., 1995). Thus, the present study demonstrates the value of using surface marine observations at

relatively high temporal frequency to better determine the climatic role of PLs in the weather conditions and sea state of the Norwegian Sea and adjacent ocean areas.

Acknowledgments

This research was funded partly by the European Community 7th framework program (FP7 2007–2013) under grant agreement 308299 (NACLIM). Support from ARISE2, a collaborative infrastructure Design Study project (2015–2018) funded by the H2020 European Commission, is also gratefully acknowledged. We thank the forecasters on duty at the Norwegian Meteorological Institute's forecasting division in Tromsø, Norway. We are grateful to D. Hauser for helpful discussions and valuable advice. We also thank the Norwegian Meteorological Institute for providing access to their data through the eklima website (<http://eklima.met.no/>). We thank the U.K.'s Natural Environment Research Council (NERC) for freely providing access to the satellite image archive. All satellite images are credited to "NERC Satellite Receiving Station, Dundee University, Scotland" (<http://www.sat.dundee.ac.uk/>). Last, we thank the reviewers for their valuable comments and suggestions that substantially improved the paper.

References

- Bowyer, P. J., & MacAfee, A. W. (2005). The theory of trapped-fetch waves with tropical cyclones—An operational perspective. *American Meteorological Society*, 20(3), 229–244. <https://doi.org/10.1175/WAF849.1>
- Carleton, A. M. (1995). On the interpretation and classification of mesoscale cyclones from satellite IR imagery. *International Journal of Remote Sensing*, 16(13), 2457–2485. <https://doi.org/10.1080/01431169508954569>
- Carleton, A. M., McMurdie, L. A., Katsaros, K. B., Zhao, H., Mognard, N. M., & Claud, C. (1995). Satellite-derived features and associated atmospheric environments of Southern Ocean mesocyclone events. *The Global Atmosphere-Ocean System*, 3, 209–248.
- Cassou, C., Terray, L., Hurrell, J. W., & Deser, C. (2004). North Atlantic winter climate regimes: Spatial asymmetry, stationarity with time and oceanic forcing. *Journal of Climate*, 17, 1055–1068.
- Claud, C., Heinemann, G., Raustein, E., & McMurdie, L. (2004). Polar Low le Cygne: Satellite observations and numerical simulations. *Quarterly Journal of the Royal Meteorological Society*, 130(598), 1075–1102. <https://doi.org/10.1256/qj.03.72>
- Claud, C., Mognard, N. M., Katsaros, K. B., Chedin, A., & Scott, N. A. (1993). Satellite observations of a polar low over the Norwegian Sea by Special Sensor Microwave/Imager, Geosat and TIROS-N Operational Vertical Sounder. *Journal of Geophysical Research*, 98(C8), 14,487–14,506. <https://doi.org/10.1029/93JC00650>
- Draper, D. W., & Long, D. G. (2004). Evaluating the effect of rain on sea winds scatterometer measurements. *Journal of Geophysical Research*, 109, C02005. <https://doi.org/10.1029/2002JC001741>
- Dysthe, K. B., & Harbitz, A. (1987). Big waves from polar lows? *Tellus*, 37A, 500–508.
- Eidsvik, K. J. (1987). Predicted hazard area for a polar low. *Tellus*, 39A(4), 390–396. <https://doi.org/10.1111/j.1600-0870.1987.tb00316.x>
- Fitch, M., & Carleton, A. M. (1991). Antarctic mesocyclone regimes from satellite and conventional data. *Tellus*, 44A, 180–196.
- Heinemann, G., & Claud, C. (1997). Report of a workshop on “theoretical and observational studies of polar lows” of the European geophysical society polar lows working group. *Bulletin of the American Meteorological Society*, 78(11), 2643–2658. <https://doi.org/10.1175/1520-0477-78.11.2643>
- Hilburn, K. A., Wentz, F. J., Smith, D. K., & Ashcroft, P. D. (2006). Correcting active scatterometer data for the effects of rain using passive microwave data. *Journal of Applied Meteorology and Climatology*, 45(3), 382–398. <https://doi.org/10.1175/JAM2357.1>
- Isachsen, P. E., Drivdal, M., Eastwood, S., Gusdal, Y., Noer, G., & Saetra, Ø. (2013). Observations of the ocean response to cold air outbreaks and polar lows over the Nordic Seas. *Geophysical Research Letters*, 40, 3667–3671. <https://doi.org/10.1002/grl.50705>
- Laffineur, T., Claud, C., Chaboureaud, J.-P., & Noer, G. (2014). Polar lows over the Nordic Seas: Improved representation in ERA-Interim compared to ERA-40 and the impact on down-scaled simulations. *Monthly Weather Review*, 142(6), 2271–2289. <https://doi.org/10.1175/MWR-D-13-00171.1>
- Mallet, P.-E., Claud, C., Cassou, C., Noer, G., & Kodera, K. (2013). Polar lows over the Nordic and Labrador Seas: Synoptic circulation patterns and associations with North Atlantic-Europe wintertime weather regimes. *Journal of Geophysical Research: Atmospheres*, 118, 2455–2472. <https://doi.org/10.1002/jgrd.50246>
- Montgomery, M. T., & Farrell, B. F. (1992). Polar low dynamics. *Journal of the Atmospheric Sciences*, 49(24), 2484–2505. [https://doi.org/10.1175/1520-0469\(1992\)049<2484:PLD>2.0.CO;2](https://doi.org/10.1175/1520-0469(1992)049<2484:PLD>2.0.CO;2)
- Moore, G. W. K., Pickart, R. S., & Renfrew, I. A. (2008). Buoy observations from the windiest location in the world ocean, Cape Farewell, Greenland. *Geophysical Research Letters*, 35, L18802. <https://doi.org/10.1029/2008GL034845>
- Noer, G., Saetra, O., Lien, T., & Gusdal, Y. (2011). A climatological study of polar lows in the Nordic Seas. *Quarterly Journal of the Royal Meteorological Society*, 137(660), 1762–1772. <https://doi.org/10.1002/qj.846>
- Nordeng, T. E. (2009). *A polar low named Vera—Dynamics and model performance*. met. no report 4/2009. Oslo, Norway: Norwegian Meteorological Institute.
- Nordeng, T. E., & Røsting, B. (2011). A polar low named Vera: The use of potential vorticity diagnostics to assess its development. *Quarterly Journal of the Royal Meteorological Society*, 137(660), 1790–1803. <https://doi.org/10.1002/qj.886>
- Oromolade, A. P., Furevik, B. R., Noer, G., Gudmestad, O. T., & Samelson, R. M. (2016). Waves in polar lows. *Journal of Geophysical Research: Oceans*, 121, 6470–6481. <https://doi.org/10.1002/2016JC012086>
- Rasmussen, E. A., & Turner, J. (2003). In E. A. Rasmussen & J. Turner (Eds.), *Polar lows: Mesoscale weather systems in the polar regions*. Cambridge: Cambridge University Press.
- Renfrew, I. A., Peterson, G. N., Sproson, D. A. J., Moore, G. W. K., & Adiwidjaja, H. (2009). A comparison of aircraft-based surface-layer observations over Denmark Strait and the Irminger Sea with meteorological analyses and QuikSCAT winds. *Quarterly Journal of the Royal Meteorological Society*, 135(645), 2046–2066. <https://doi.org/10.1002/qj.444>
- Rojo, M., Claud, C., Mallet, P.-E., Noer, G., Carleton, A. M., & Vicomte, M. (2015). Polar low tracks over the Nordic Seas: A 14-winter climatic analysis. *Tellus*, 67(1). <https://doi.org/10.3402/Tellusa.v67.24660>
- Saetra, O., Linders, T., & Debernard, J. B. (2008). Can polar lows lead to warming of the ocean surface? *Tellus*, 60A, 141–153.
- Weissman, D. E., & Bourassa, M. A. (2008). Measurements of the effect of rain-induced sea surface roughness on the QuikSCAT scatterometer radar cross section. *IEEE Transactions on Geoscience and Remote Sensing*, 46(10), 2882–2894. <https://doi.org/10.1109/TGRS.2008.2001032>
- Weissman, D. E., Stiles, B. W., Hristova-Veleva, S. M., Long, D. G., Smith, D. K., Hilburn, K. A., & Jones, W. L. (2012). Challenges to satellite sensors of ocean winds: Addressing precipitation effects. *Journal of Atmospheric and Oceanic Technology*, 29(3), 356–374. <https://doi.org/10.1175/JTECH-D-11-00054.1>
- Zappa, G., Shaffrey, L., & Hodges, K. (2014). Can polar lows be objectively identified and tracked in the ECMWF operational analysis and the ERA-Interim reanalysis? *Monthly Weather Review*, 142(8), 2596–2608. <https://doi.org/10.1175/MWR-D-14-00064.1>